Reprinted from LANGMUIR, 1994, 10.

Dispersions of Rhodamine-Labeled Silica Spheres: Synthesis, Characterization, and Fluorescence Confocal Scanning Laser Microscopy

Nynke A. M. Verhaegh* and Alfons van Blaaderen

Van't Hoff Laboratory, University of Utrecht, Padualaan 8, 3584 CH Utrecht, The Netherlands

Received July 28, 1993. In Final Form: December 27, 1993®

Monodisperse colloidal silica spheres, with a total radius of 200 nm, labeled with the fluorescent dye rhodamine isothiocyanate (RITC) in a core of 100 nm radius have been synthesized. The particles were characterized by transmission electron microscopy and by static and dynamic light scattering. The fluorescence properties and dye concentration in the particles were measured with fluorescence and absorption spectroscopy. Stable dispersions of these hydrophilic, charge-stabilized silica spheres in polar solvents and of organophilic, sterically stabilized, 1-octadecanol-coated silica spheres in apolar solvents were studied with fluorescence confocal scanning laser microscopy (CSLM). The bleachability of these particles was determined with CSLM and compared with particles labeled with the dye fluorescein isothiocyanate (FITC). The possibilities and limitations of confocal microscopy to study individual fluorescent particles in the bulk of concentrated model dispersions are discussed and demonstrated with CSLM graphs of a time series showing colloidal crystallization (crystal growth rate approximately 4 μm/s), an equilibrium between a colloidal liquid and colloidal crystal interface, and a binary mixture of RITC- and FITC-labeled spheres. Further, the feasibility of using the RITC-labeled spheres with other techniques relying on fluorescence is discussed as well.

1. Introduction

Several experimental techniques to study the structure and dynamics of dispersions rely in one way or another on fluorescence, e.g. *fluorescence* recovery after photobleaching (FRAP[1]), *fluorescence* correlation spectroscopy (FCS[2]), *fluorescence* cross correlation spectroscopy using two dyes,[3] and *fluorescence* confocal scanning laser microscopy (CSLM[4,5]). For all these techniques the availability of well-characterized fluorescent model particles is essential.

Recently, we succeeded in synthesizing fluorescein isothiocyanate (FITC) labeled silica spheres.[6] The fluorescent dye was covalently bound to a coupling agent, which participated in the synthesis of monodisperse silica spheres by a modification of the process developed by Stöber *et al.*[7] This resulted in organosilica spheres in which the organic dye is distributed homogeneously. Onto this core an outer shell of nonfluorescent silica was grown. The particles so obtained are excellent model particles, because the dye can never leave the particle (see, e.g., ref 3) and does not influence the interparticle potential since it is far away from the particle surface. Furthermore, the refractive index of the silica particles is close to that of apolar solvents in which they can be dispersed after a coating reaction with 1-octadecanol, which provides steric stabilization.[8] This refractive index matching makes it possible to prepare concentrated (>50% volume fraction) dispersions of large particles that are hardly turbid.[9] Charged silica spheres can be matched and studied in the polar solvent dimethylformamide.

FITC-labeled silica spheres have been studied by fluorescence confocal scanning laser microscopy.[9,10] With CSLM it is possible to image individual particles in the bulk of a concentrated dispersion, due to a combination of a powerful depth discrimination (optical sectioning) and an increased resolution compared to conventional light microscopy. Both properties are a consequence of the extremely limited field of view of CSLM. Only a diffraction limited point is focused inside the specimen and the fluorescence intensity is subsequently imaged on a point detector.[11] Consequently, the image has to be built up by scanning. Typically, the digital construction of an image plane of 512 by 768 pixels takes about 1 s. With an excitation wavelength of 488 nm for the dye FITC and a lens with numerical aperture (N.A.) 1.3, a lateral resolution of 0.2 μm (both in x and y direction) and an axial resolution of 0.65 μm are possible.[11] With the stored data of several parallel cross sections, a 3-D image can be constructed by digital image analysis. A short discussion on the advantages of CSLM compared to conventional directly imaging methods of colloidal particles in concentrated dispersions is given in ref 9.

The vulnerability of the fluorophore FITC to photobleaching impedes CSLM measurements (though it is essential for FRAP measurements[12]); therefore, a new fluorescent silica system was prepared, labeled with another dye, which would make the system better suited for CSLM studies. For this purpose, the dye rhodamine isothiocyanate (RITC) was chosen, since it is reported to be less bleachable than FITC[13,14] and since its fluorescence characteristics supplement those of FITC very well.[13] Free RITC in a mixture of ethanol, ammonia, and water has its excitation and emission maxima at 546 and 568 nm,

® Abstract published in *Advance ACS Abstracts,* March 1, 1994.

(1) Davoust, J.; Devaux, P.; Leger, L. *EMBO J.* **1982**, *1*, 1233.
(2) Drewel, M.; Pusey, P. N. *Opt. Acta* **1983**, *30* (10), 1483.
(3) Ricka, J.; Binkert, T. *Phys. Rev. A* **1989**, *39* (5), 2646.
(4) Wilson, T. *J. Phys. E: Sci. Instrum.* **1989**, *22*, 532.
(5) Brakenhoff, G. J.; van der Voort, H. T. M.; van Spronsen, E. A.; Nanninga, N. *Scanning Microsc.* **1988**, *2* (1), 33.
(6) van Blaaderen, A.; Vrij, A. *Langmuir* **1992**, *8*, 2921.
(7) Stöber, W.; Fink, A.; Bohn, E. *J. Colloid Interface Sci.* **1968**, *26* (1), 62.
(8) van Helden, A. K.; Jansen, J. W.; Vrij, A. *J. Colloid Interface Sci.* **1981**, *81* (2), 354.
(9) van Blaaderen, A. *Adv. Mater.* **1993**, *5* (1), 52.
(10) van Blaaderen, A.; Imhof, A.; Hage, W.; Vrij, A. *Langmuir* **1992**, *8* (6), 1514.
(11) Wilson, T. *Confocal Microscopy*; Academic Press: London, 1990.
(12) van Blaaderen, A.; Peetermans, J.; Maret, G.; Dhont, J. K. G. *J. Chem. Phys.* **1992**, *96* (9), 4591.
(13) Lakowicz, J. R. *Principles of Fluorescence Spectroscopy*; Plenum Press: New York, 1984.
(14) Nairn, R. C. *Fluorescent Protein Tracing*, 4th ed.; Churchill Livingstone: Edingburgh, 1976.

0743-7463/94/2410-1427$04.50/0

respectively. Free FITC in the same mixture has its excitation and emission maxima at 501 and 526 nm, respectively.[6] Since the fluorescence characteristics of both dyes are distinguishable, it is possible to study binary mixtures consisting of spheres labeled with either FITC or RITC, in a CSLM set up that excites and detects both fluorophores simultaneously.

The radius of the fluorescent core was chosen close to 100 nm and that of the total radius around 200 nm. The size of the silica layer is a consequence of the following: first, the necessity to have particles with a thick silica layer, so that they become monodisperse and that the size of the nonfluorescent intercore distance is large enough to allow distinction of neighboring particles by CSLM; second, the necessity to have spheres with limited sedimentation rate and (for sterically stabilized spheres) limited van der Waals forces. The size of the core was as small as possible for this method of synthesis.

In this paper we describe the synthesis and extensive characterization of these RITC labeled silica spheres. The charge stabilized spheres were dispersed in polar solvents, and after a coating reaction with 1-octadecanol the sterically stabilized spheres were dispersed in several apolar solvents. Size and polydispersity of the particles were measured with transmission electron microscopy and static and dynamic light scattering. The amount of dye incorporated, particle density, and refractive index were determined. The fluorescence emission and excitation of RITC inside the silica particles were measured, and the bleachability of RITC and FITC labeled spheres was compared by CSLM measurements.

Finally, CSLM micrographs of dispersions of the RITC labeled spheres in chloroform are presented. The technique was ideally suited to study both the dynamics of crystallization and the structure of the crystalline phase in this colloidal system. Further, a bimodal system containing large FITC labeled spheres and smaller RITC labeled spheres in chloroform was studied with dual excitation and detection. The spatial distribution of the two kinds of spheres was revealed by CSLM, both before and after colloidal crystallization.

2. Experimental Section

A. Materials. The solvents hexadecane (99%, Janssen), 1-propanol (Janssen), toluene (Baker), chloroform (Baker), tetrachloromethane (tetra, Baker), cyclohexane (Janssen), *N*,*N*-dimethylformamide (DMF, 99%, Janssen), and ammonium hydroxide (ammonia, Merck, 25%) were of analytical reagent quality. The ammonium hydroxide, which will subsequently be referred to as "ammonia", contained 14.8 M NH_3 as was determined by titration. Hydrofluoric acid was obtained from Merck (38–40%, extra pure). Ethanol (absolute technical grade, Nedalco) was used after distillation. The reagents tetraethoxysilane (TES, Fluka, purum grade) and (3-aminopropyl)triethoxysilane (APS, 99%, Janssen) were freshly distilled before the synthesis. Sodium hydroxide pellets (Merck, zur synthese), 1-octadecanol (stearyl alcohol, Merck, zur synthese), and rhodamine B isothiocyanate (RITC mixed isomers, Fluka) were used as received.

B. Particle Synthesis. The rhodamine labeled particles were synthesized according to the procedure described by van Blaaderen *et al.* for organosilica spheres.[6] This synthesis will be described concisely, emphasizing the differences. Note that color effects described here are due to absorbance and light scattering as well as fluorescence. They are subjective observations, mentioned only to indicate possible changes. Fluorescence was observed under illumination with a UV lamp. Filters were used, in order to distinguish fluorescence from light scattering.

All glass reaction vessels were cleaned extensively to ensure that no nucleation sites were present (washing procedure: filling with 8% hydrofluoric acid (HF) for half an hour; removing HF by subsequently rinsing with cold, hot, and deionized water; finally rinsing with distilled ethanol).

In a reaction vessel, which had been dried for 3 h at 120 °C, 0.0938 g of the coupling agent APS (4.25×10^{-4} mol) was added to 0.1178 g of the fluorophore RITC (2.20×10^{-4} mol) in a medium of 10 mL of anhydrous ethanol. The reaction proceeded for 17 h in the dark with magnetic stirring and under nitrogen. The color of the solution was dark purple, and due to strong self-quenching orange fluorescence could only be observed at the edges. The small surplus of APS was required to avoid a possible loss of RITC by a reaction with ammonia during further steps. By adding free RITC to an alcosol, we determined that the dye did not adsorb onto silica and thus changed the surface charge of the spheres: after centrifugation the sediment was white and the supernatant was red.

The organosilica cores were synthesized under nitrogen in 670 mL of ethanol and 51 mL of ammonia (final concentrations, 1 M NH_3 and 2.8 M H_2O). Reagent concentrations were chosen to prepare spheres with a radius of about 100 nm.[8,15] The coupled dye (APS-RITC) was quantitatively transferred into the reaction vessel under mechanical stirring, resulting in a dark red, transparent mixture with orange fluorescence. The reaction vessel was thermostated at 21.5 °C. The reagent TES (28.3 mL, 0.127 mol) was added by a funnel under the solution surface and under severe mechanical stirring.

After a few minutes the solution became turbid, and the stir rate was decreased. After $5^1/_2$ h a small fraction of fluorescent organosilica core particles (CORE) was isolated. The growth steps were executed in the original reaction mixture, to prevent particle aggregation by centrifugation. Consequently, there was still dye present in the supernatant which had not been incorporated, as could be seen after centrifuging a small fraction of the dispersion. Although the supernatant remained colored by RITC during all growth steps, the final particles had a fluorescent core only. Apparently, the presence of the dye did not disturb the coating with silica.

First, only 0.7 mL of TES was added to deposit a thin layer of silica on the particles and to prevent flocculation by increasing the ionic strength too much.[16] After that a total amount of 253 mL of TES was added in larger portions with intervals of at least 2 h. Water was regularly added as well, to maintain the molar ratio water:TES at least 10:1. The final radius was theoretically predicted to be 203 nm, based on the amount of TES added.[6]

The final volume of the reaction mixture was centrifuged at 900 rpm in a Beckman L5-50B ultracentrifuge for 2 h. The sediment showed crystal reflections in the top layer. A stable dispersion in a fresh mixture of ethanol and ammonia (1 M NH_3 and 2.8 M H_2O) was prepared which will be referred to as "SISOL".

For the esterification of the alcosol with 1-octadecanol, as described by van Helden,[8] 215 g of stearyl alcohol was dissolved in 500 mL of ethanol under magnetic stirring at 70 °C. A volume of the alcosol containing approximately 43 g of silica was added in three portions. Ammonia and ethanol were removed by distillation. The excess of water was removed by azeotropic distillation by adding 250 mL of propanol in two portions. The temperature of the remaining melt of 1-octadecanol was gradually increased to 150 °C, after which the reaction mixture was placed under a dry nitrogen flow. Finally, the temperature was stabilized at 190 °C, where the esterification took place during 16 h. Once coated with 1-octadecanol, the silica particles form a gel phase in the liquid 1-octadecanol at temperatures around its melting point. Therefore, the mixture was left in an oven at 80 °C for 48 h. Almost all stearyl alcohol, which was vaguely colored red, could be decanted and, finally, the coated silica spheres were washed in chloroform and in cyclohexane both by 3 times centrifugation. The rhodamine-labeled, stearyl-coated silica spheres, which will be referred to as "STSI", seemed darker red than the uncoated ones (SISOL), because the refractive index of the silica spheres was matched better in apolar solvents. Visually, no difference could be observed in the fluorescence color of STSI and SISOL (see also section 3B).

(15) Bogush, G. H.; Tracy, M. A.; Zukoski, C. F., IV *J. Non-Cryst. Solids.* **1988**, *104*, 95.

(16) van Blaaderen, A.; van Geest, J.; Vrij, A. *J. Colloid Interface Sci.* **1992**, *154* (2), 481.

Table 1. Characteristics of Binary Mixtures Dispersed in Chloroform (4F-s/STSI) and in Dimethylformamide (FSA 7(3)/SISOL)[a]

4F-s/STSI ($CHCl_3$)	R_{core}	R	ϕ	n	FSA 7(3)/SISOL (DMF)	R_{core}	R	ϕ	n
STSI (RITC)	100	215	0.3%	1	SISOL (RITC)	100	215	50%	1
4F-s (FITC)	195	492	25%	7	FSA 7(3)(FITC)	180	200	50%	1

[a] R_{core} is the radius of the fluorescent core, R is the radius of the silica sphere, ϕ is the volume fraction, and n indicates the number ratio. The fluorescein-labeled spheres (4F-s and FSA 7(3)) are reproduced from refs 6 and 17.

Dispersions in several solvents were prepared by successive centrifugation and replacement of the supernatant.

A binary mixture of the rhodamine-labeled STSI and fluorescein-labeled silica spheres 4F-s described by van Blaaderen[6] was made in chloroform, and this will be referred to as "4F-s/STSI". Another binary mixture of SISOL and fluorescein-labeled silica spheres FSA 7(3)[17] was made in dimethylformamide, and this will be referred to as "FSA 7(3)/SISOL". The characteristics of both binary mixtures are presented in Table 1.

C. Particle Characterization. *Particle Radius.* Transmission electron microscopy (TEM) results were obtained on a Philips CM10 transmission electron microscope (100 keV). A diffraction grating was used to calibrate the magnification. Copper 400-mesh carrier grids, covered with carbon-coated Formvar films, were dipped into dilute dispersions, and the particles retained on the film were observed. The TEM negatives were studied with an interactive image analysis system. Hundreds of particles were analyzed, and based on the surface area a number average particle radius and its standard deviation were determined (Gaussian distribution). These were used to calculate the polydispersity (δ) of the system ($\delta = \sigma_{n-1}/\langle R \rangle$).

For the scattering measurements dilute samples were filtered through Millipore filters into glass cuvettes, rinsed with freshly distilled acetone, to obtain dust-free samples. Static light scattering (SLS) results were obtained from dispersions in ethanol with a Fica-50 photometer using vertically polarized light, both for the incident and detected beam, at 24.5 °C. Scattering was measured at 365, 436, 546, and 578 nm. Antifluorescence filters were used for 365, 436, and 546 nm. Intensities were obtained in the range of $25° \leq \theta \leq 140°$ (θ = scattering angle). The optical radius was determined by fitting experimental curves to theoretical curves based on a calculation of Mie scattering coefficients taking polydispersity into account.[18,19] The wavelength dependence of the refractive index of the particles can be neglected,[20] and this was also demonstrated experimentally in the next section. The refractive index of the solvent was corrected for wavelength using the "dispersion coefficient" which was measured on a thermostated Abbe refractometer.

Dynamic light scattering (DLS) measurements were performed with a Spectra Physics Series 2020 krypton laser operating at a wavelength of 647.1 nm. This wavelength was chosen because it is not absorbed by rhodamine and therefore convection caused by heating of the spheres, will not disturb the measurements. Normalized time autocorrelation functions were measured with a Malvern Multi 8 7032 CE 128 points correlator. Diffusion coefficients were obtained from cumulant fits[21,22] of autocorrelation functions at scattering angles between 35° and 79°. From diffusion coefficients the hydrodynamic radius was calculated using the Stokes–Einstein relation.[23]

Particle Density and Refractive Index. The mass fraction of a dispersion was determined by weighing a few milliliters in an aluminum cup. The solvent was evaporated in a sample concentrator under a nitrogen flow at 80 °C for 2 days. The aluminum cup containing the silica residue was weighed again to determine the mass fraction of silica.

In order to determine the particle density, a known volume of solvent was weighed to determine its density. The same volume, filled with a dispersion of STSI in the same solvent with known mass percentage, was weighed. The volume of the solvent fraction was calculated, using its density. The density of the silica could then be determined by dividing the silica mass by the silica volume, assuming no volume contraction.

The mean refractive index of a dilute dispersion of silica spheres equals the refractive index of the solvent at that temperature where the transmission is at a maximum. Therefore, the transmission as a function of temperature was measured for a silica dispersion both in chloroform and in tetrachloromethane with a Shimadzu double beam (Spectronic 200 UV) spectrophotometer. The transmission was followed at 554 and 647 nm, the maximum in absorption for the rhodamine labeled spheres and a wavelength at which no absorption occurs. It is assumed that the refractive index of the silica spheres is to a first approximation independent of temperature.[20] The absorption measurements were performed at low volume fraction (0.1%).

Fluorescence and Absorption Spectroscopy. Fluorescence emission and excitation spectra of rhodamine labeled silica spheres were recorded with a SPF-500C spectrofluorometer. For recording of the emission spectra the dye was excited at 500 nm, and the emission of the excitation spectra was detected at 600 nm. The absorption was measured with a Hewlett-Packard 8452 A diode array spectrophotometer. Analogously to the procedure described by Giesche *et al.*,[24] a known volume of a SISOL dispersion in ethanol was dissolved in a basic sodium hydroxide solution (0.4 M NaOH). The silica dissolved and the rhodamine concentration present in the silica spheres was determined spectrophotometrically.

D. Fluorescence Confocal Scanning Laser Microscopy (CSLM) and Bleachability. Confocal laser-scanned images were obtained with a Biorad MRC 600 equipped with a combined krypton/argon mixed gas laser mounted on a Zeiss Axioplan. The lines used were 488 and 568 nm, and optionally both lines could be used simultaneously (dual excitation).

Dispersions containing only rhodamine-labeled particles were measured with the YHS filter block (Biorad), containing a dichroic reflector (*DR 585 LP*). This filter block allows excitation at 568 nm (exciter filter *568 DF 10*) and detection of the fluorescence above 585 nm (emission filter *585 EFLP*). Dual excitation was performed with a K1 filter block (Biorad) containing a *K1 double dichroic* reflector, which allows excitation of FITC with 488 nm (transmission window between 480 and 490 nm) and RITC with 568 nm (transmission window between 555 and 580 nm). Dual detection was performed with a K2 filter block (Biorad) containing a *K2 dichroic 560 LP* reflector. This filter block allows detection of wavelengths between 500 and 585 nm on one photonmultiplier tube (PMT: FITC channel; emission filter *522 DF 32*) and detection of wavelengths above 585 nm on the other PMT (RITC channel: emission filter *585 EFLP*; see also section 3B).

Objectives used were 40× and 63×, 1.3 and 1.4 N.A. oil immersion lenses. Images of transverse cross sections were obtained by optical scanning. The *z*-axis drive from Biorad was modified to drive the focus of the stage. Samples were measured in flat glass capillaries (Vitro Dynamics: thickness, 100 and 200 μm; width, respectively, 1 and 2 mm), sealed off by melting.

A binary mixture of rhodamine-labeled SISOL and fluorescein-labeled FSA 7(3) (R_{CORE} = 180 nm and R_{final} = 200 nm, see ref 17) in dimethylformamide (FSA 7(3)/SISOL) and dispersions of the unmixed particles in DMF were studied with CSLM to compare the bleachabilities of both fluorophores. To make sure that the charge-stabilized particles were immobile, a glassy

(17) Imhof, A. To be submitted for publication.

(18) Bohren, C. F.; Huffman, D. R. *Absorption and scattering of light by small particles*; John Wiley & Sons: New York, 1983.

(19) Kerker, M. *Scattering of light and other electromagnetic radiation*; Academic Press: New York, 1969.

(20) Pathmamanoharan, C.; Kops-Werkhoven, M. M. *Chem. Phys. Lett.* **1982**, *93* (4), 396.

(21) Koppel, D. E. J. *J. Chem. Phys.* **1972**, *57*, 4814.

(22) van Veluwen, A.; Lekkerkerker, H. N. W.; de Kruif, C. G.; Vrij, A. *J. Chem. Phys.* **1988**, *89* (5), 2810.

(23) *Dynamic light scattering: Applications of photon correlation spectroscopy*; Pecora, R., Ed.; Plenum Press: New York, 1985.

(24) Giesche, H.; Matijévic, H. G. E. *Dyes Pigm.* **1991**, *17*, 323.

sediment in a capillary was made by centrifuging at 3000 rpm. A line scan of the sediment close to the glass wall was made parallel to the capillary. Both single and dual excitation options were used, the latter in order to expose the dyes to equal intensity. The intensity of the laser beams was about 5 mW for each wavelength (Biorad). Each line scan consisted of 768 pixels and typically the time necessary for performing one line scan was 2 ms. Subsequently, 512 successive scans were made of the same line so that the observed line could be studied as a function of time. By averaging each line scan over an adjustable number of times, the total exposure time was varied. Each line scan contained information on the position of the fluorescent spheres in the studied part of the specimen, since each line scan consisted of a pattern of bright and dark regions. The bleachability was assessed by examining the fluorescent intensity of a small region of the line as a function of exposure time, i.e. the intensity of the same region of the line was recorded for all successive line scans. This small region of the line scan over which the intensity was recorded was 15 pixels wide (equivalent to 740 nm). The size of this region was chosen such that it contained one bright spot, correlated to one fluorescent sphere. Averaging over a different number of pixels did not change the results. By depicting the 512 successive line scans parallel to each other, a picture frame was filled, making it possible to check that the same part of the specimen was bleached. This was necessary because sometimes a movement of the sample of several micrometers was observed parallel to the direction of the line scan. Therefore, only a small region of the line scan has been analyzed for bleaching, which was recognizable in the sequence of line scans, so that we were able to correct for the movement of the sample. Possible explanations for the observed movement are internal movement of the microscope or an anisotropic expansion of the capillary due to local heating.

3. Results and Discussion

A. Particle Synthesis and Characterization. The molar ratio TES:RITC in the synthesis of fluorescent CORE particles was 580:1. This ratio was chosen because it is known that the fluorescence intensity increases linearly with the fluorophore concentration, until a certain concentration is reached. Starting from this concentration, the slope of fluorescence intensity versus concentration becomes smaller and may even change sign, for instance due to an extra transition of excited electrons to the ground state, without emission of photons (self-quenching[13]). Therefore, tests were performed to determine the concentration dependence of the fluorescence intensity of rhodamine-labeled organosilica cores. The ratio TES:RITC was varied for several organosilica core syntheses. Visually, fluorescence intensities have been compared and the self-quenching point of RITC appeared to be situated somewhere between the molar ratios TES:RITC = 450:1 and 700:1.

During the synthesis and the growth procedure the reaction mixture was stable and turbid. The dispersion was colored pink and the fluorescence was orange. Small fractions isolated at various states of the growth procedure were left to sediment undisturbed, leading to pink sediments and red transparent supernatants, both with orange fluorescence. Obviously, the RITC was still not completely incorporated after all the growth steps. Since it has been concluded that the free dye did not adsorb onto the particles, only the dye coupled to APS ended up inside the particles. Based on earlier studies it is expected that such small concentrations of APS as used here would be incorporated almost completely.[16] Therefore, the dye which was still in the supernatant after growing of the spheres with silica up to their final size, was probably not chemically bound to APS. Consequently, it is likely that the initial reaction between APS and RITC had not been completed. Further work on this reaction is, however, required to verify this conclusion and to find an explanation for it.

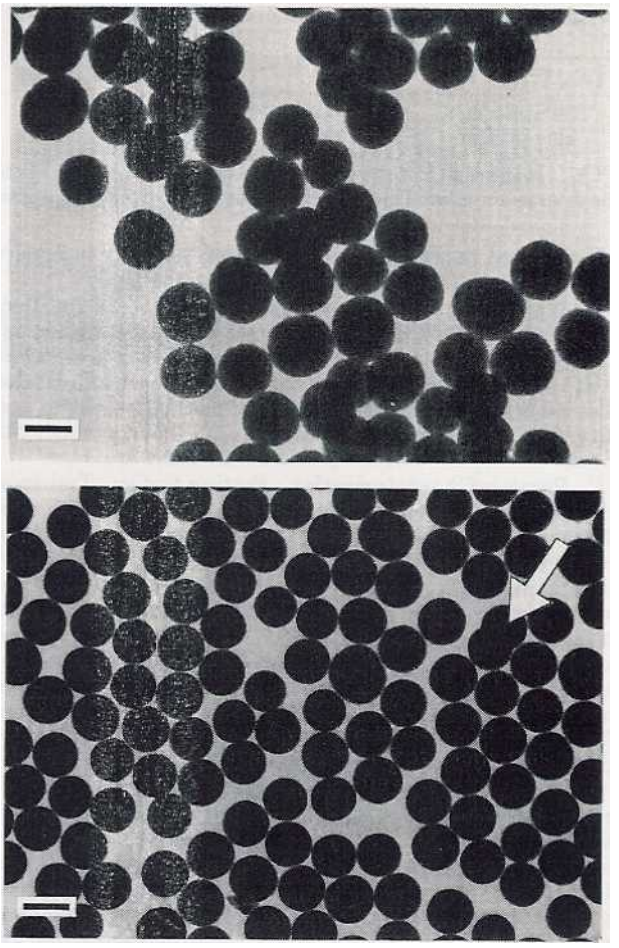

Figure 1. Transmission electron micrographs of (a, top) CORE particles with R_{EM} = 92.3 nm and δ = 10.7% (bar = 150 nm) and (b, bottom) STSI particles with R_{EM} = 195 nm and δ = 5.5% (bar = 400 nm). In Figure 1b the arrow points at a dumbbell.

The STSI fraction dispersed in cyclohexane and chloroform showed no crystal reflections after centrifugation at rotation rates between 1000 and 2500 rpm. After sedimentation by gravity, reflections could be observed in the sediments, indicating crystallinity. The appearance of crystallites is in accordance with an unclustered and monodisperse dispersion.[25]

Particle Radius. The radii of the organosilica CORES coated with a thin layer of silica (calculated to be 0.3 nm), and the radii of the SISOL and STSI particles, as obtained by TEM, SLS, and DLS, are summarized in Table 2. In this table the theoretically predicted radii, based on the starting concentrations of water and ammonia for the CORE[8,15] and on the amount of TES added for SISOL and STSI,[16] are included as well. For completeness the radii of the fluorescein-labeled spheres are reproduced from refs 6 and 17.

Figure 1a shows an electron micrograph of the CORE particles after a coating with a thin layer of silica (Table 2, 0.3 nm calculated[16]). The organosilica CORES are rather spherical; the polydispersity is 10.7%, which is somewhat higher than for pure silica particles of similar size.[8,15] This is probably due to the presence of RITC-APS at the start of the particle synthesis.

(25) Davis, K. E.; Russel, W. B.; Glantschnig, W. J. *J. Chem. Soc., Faraday Trans.* **1991**, *87* (3), 411.

Table 2. Particle Radii and Polydispersities (δ) of Rhodamine-Labeled Silica Spheres (CORE, SISOL, and STSI), As Obtained by Transmission Electron Microscopy (R_{TEM}), Static Light Scattering (R_{SLS}), Dynamic Light Scattering (R_{DLS}), and Theoretically Calculated (R_{th})[a]

system	R_{th} (nm)	R_{TEM} (nm)	δ (%)	R_{SLS} (nm)	R_{DLS} (nm)
CORE	101	92.3	10.7	100	100
SISOL	203	188		215	201
STSI	203	195	5.5		207
Core of 4F-s		195	5	210	202
4F-s		492	1.9		490
FSA 7(3)		179	5.5	200	188

[a] The data for the fluorescein-labeled spheres (4D, 4F-s, FSA 7(3)) are reproduced from refs 6 and 17.

In Figure 1b an electron micrograph of the STSI particles is shown, which contains almost perfectly spherical particles with smooth surfaces and a narrow size distribution ($\delta = 5.5\%$). The sterically stabilized particles have arranged themselves in almost hexagonal order during evaporation of the solvent. The arrow points at a dumbbell particle. Apparently, a small fraction of the CORE particles grew together during the growth step due to an increase in ionic strength after addition of TES.[6] The TEM radii are somewhat smaller than the light scattering radii. Such a difference has been observed often for this kind of system. It is ascribed to shrinkage of the spheres caused by electron beam damage in the TEM microscope.[8]

The optical radius was determined only with static light scattering in ethanol, because the refractive index of the apolar solvents cyclohexane and chloroform is too close to that of the particles to measure an interpretable particle form factor.[26] The scattering curves as a function of the scattering vector $\vec{K}$ for the organosilica CORES are presented in Figure 2. The magnitude of the scattering vector is given by:

$$K = \frac{4\pi n \sin\frac{\theta}{2}}{\lambda_0} \qquad (1)$$

in which θ is the scattering angle, n is the refractive index of the dispersion, and λ_0 is the wavelength in vacuum.

As can be seen in Figure 2 the form factors obtained at the different wavelengths superimpose with the theoretical Mie scattering curve for a radius of 100 nm, assuming a Gaussian polydispersity of 10% as determined by TEM, except for a slight upward deviation at small scattering vectors. However, at 436 nm RITC inside the particles hardly absorbs light and at 546 nm the absorption is almost at a maximum (section 3B). Obviously, no effect of the dye on the scattering is observed. A calculation of the complex part of the particle refractive index gives a q value of 2.6×10^{-4} (section 3B), which is too low indeed to cause any effect on the scattering.

The slight upward deviation at small scattering vectors is probably due to some clustering of the CORE particles. The SLS measurements were performed several weeks after the synthesis and it is known that particles with APS on their surface are less stable than pure silica particles.[16] The SISOL particles did not have any deviation at small K. Obviously, only very few dumbbells have been formed. With a polydispersity of 5.5% (Table 1) a radius of 215 nm was obtained.

Diffusion coefficients determined with DLS are shown in Figure 3 as a function of the scattering vector. The DLS radii inserted in Table 1 were derived from the average diffusion coefficient. No angle dependence of the diffusion coefficients is observed and the normalized cumulant fits

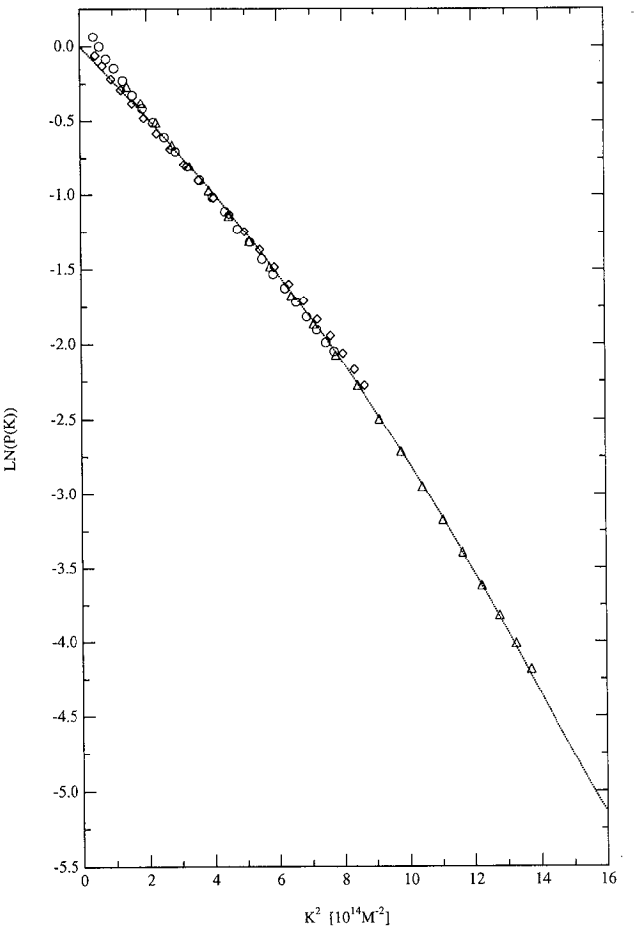

Figure 2. Static light scattering curves ($\ln(P(K))$ vs K^2) for the fluorescent CORE particles measured at 436 (△), 546 (◇), and 578 nm (○) together with a Mie scattering curve for $R = 100$ nm, assuming a Gaussian polydispersity of 10%. The experimental curves at 436 and 546 nm are measured with antifluorescence filters. The dashed line represents the Mie scattering curve.

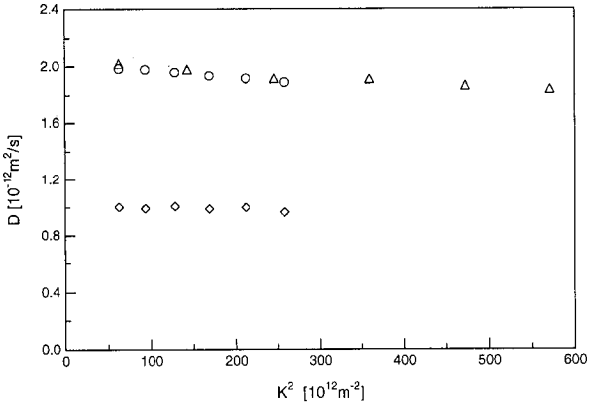

Figure 3. Diffusion coefficients obtained with dynamic light scattering (D) versus K^2 for silica spheres doped with RITC: ○, STSI in $CHCl_3$; ◇, SISOL in EtOH; △, CORE in EtOH.

were smaller than 0.05. Both are indications of unclustered, monodisperse dispersions.

Particle Refractive Index, Density, and Dye Content. For the determination of the mean refractive index of the particles, it was chosen to change the solvent refractive index by varying the temperature. In this way preferential absorption is avoided which can occur by changing the solvent composition.[26] Transmission changed only slightly

(26) van Helden, A. K.; Vrij, A. *J. Colloid Interface Sci.* **1980**, *76* (2), 418.

Table 3. Excitation and Emission Maxima of Free RITC and FITC and Rhodamine- and Fluorescein-Labeled Particles[a]

system	solvent	concentration	λ_{exc} (nm)	λ_{em} (nm)
RITC	ethanol/ammonia (14.8 M)/water (41.7 M)	5.4 g/L	546	568
SISOL	ethanol/ammonia (14.8 M)/water (41.7 M)	2.6×10^{-2} vol %	564	580
STSI	cyclohexane	1.6×10^{-1} vol %	560	575
FITC	ethanol/ammonia (100:8 (v/v))	10^{-5} g/L	501	526
2C	ethanol/ammonia (100:8 (v/v))	5×10^{-3} vol %	500	519
2C-s	cyclohexane	5×10^{-3} vol %	525	535, 385

[a] Data of free FITC and FITC-labeled spheres are reproduced from ref 6.

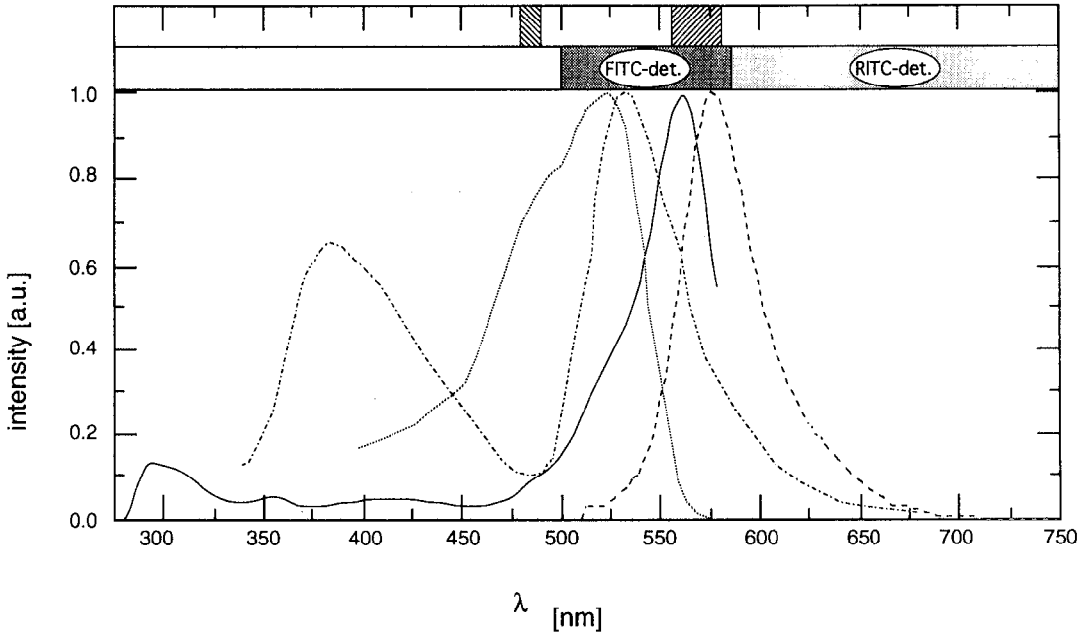

Figure 4. Fluorescence excitation and emission spectra of STSI in cyclohexane (1.6×10^{-1} vol %: excitation, drawn line; emission, dashed line) and 2C-s in chloroform (5×10^{-3} vol %: excitation, dotted line; emission, dot-dashed line). The excitation wavelength is 500 nm for RITC and 310 nm for FITC, and the emission wavelength is 600 nm both for RITC and FITC. The upper bar shows the ranges of excitation for FITC (hatched with negative slope, around 488 nm) and for RITC (hatched with positive slope, around 568 nm). In the lower bar the dark gray area represents the band-pass filter between 500 and 585 nm, as is used for detection of FITC, and the light gray area represents a long pass filter starting at 585 nm, as is used for detection of RITC.

with temperature, because the particles were almost matched in the solvents chloroform and tetrachloromethane. A dispersion of STSI in tetrachloromethane had its transmission maximum for $\lambda = 647$ nm at 37.4 ± 0.2 °C corresponding to a refractive index of 1.448. The same particles dispersed in chloroform gave a transmission maximum for $\lambda = 647$ nm at 13.2 ± 0.5 °C, corresponding to $n_D = 1.446$. In chloroform the particle refractive index was also measured at the absorption maximum of the dye in the particles ($\lambda = 554$ nm), revealing an n_D of 1.449 (17.3 ± 0.2 °C). These values are as expected when the dye does not noticeably influence the particle refractive index (e.g. ref 6).

The density of STSI was determined to be 1.88 g/mL at room temperature, also in accordance with earlier findings.[6] The dye content was determined spectrophotometrically after dissolution of SISOL in 0.4 M NaOH. The extinction coefficient of RITC in such a solution was determined to be 6.2×10^6 $(M \cdot m)^{-1}$. The concentration of dye was determined to be 2.7×10^{-3} mol of fluorophore/L of silica (6.6×10^4 molecules of fluorophore per particle; see Table 4). From these values an incorporation efficiency of 49% of the RITC used in the synthesis was calculated. Assuming a homogeneous distribution of the dye molecules in the CORE particles an intermolecular distance of 4 nm is obtained. This distance is somewhat larger than the molecule itself, though of the same order of magnitude. Therefore, this value agrees with the observation that the molar TES:RITC ratio is close to its self-quenching point (see above).

B. Fluorescence and Bleachability. The excitation and emission maxima of free RITC and FITC and the dyes incorporated in silica spheres are displayed in Table 3. The normalized fluorescence spectra for STSI and FITC labeled 2C-s particles[6] are given in Figure 4. In the top part of Figure 4 some characteristics are displayed of the CSLM setup used with the dual excitation option. The hatched ranges in the upper band indicate the range of excitation wavelengths for FITC (480–490 nm) and RITC (555–580 nm). In the lower band the dark gray area represents the detection window for FITC (band–pass filter between 500 and 585 nm) and the light gray area the detection window for RITC (long pass filter starting from 585 nm).

From the figure it follows that the excitation wavelength is almost perfect for rhodamine inside stearyl-coated silica and that it is somewhat less optimal, but still very close to the maximum excitation, for fluorescein in stearyl-coated silica. For the fluorescence detection the situation is reversed: here the detection window for the FITC-labeled silica spheres is almost optimal and somewhat less for the RITC-labeled spheres. However, a large part of the rhodamine fluorescence is still detected. From the figure it also follows that some emission of RITC can be detected in the detection window of the FITC detector and vice versa also some emission of FITC can be detected on the RITC channel. In order to obtain an improved separation of the two fluorophores, methods have been

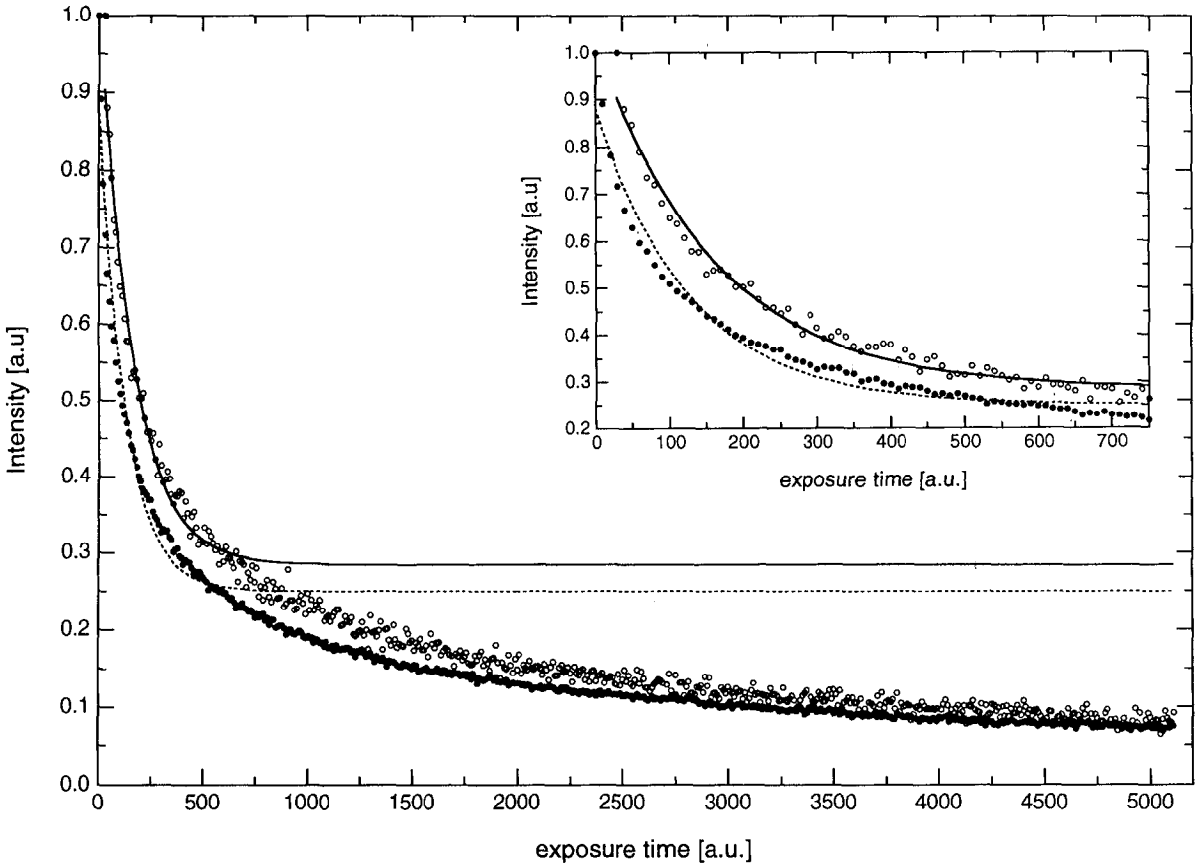

Figure 5. Fluorescence intensity versus exposure time for RITC-labeled spheres (SISOL, dark circles) and FITC-labeled spheres (FSA 7(3), open circles). The data were obtained with dual excitation (488 and 568 nm) and dual detection of the binary mixture FSA 7(3)/SISOL. The drawn and dashed lines are single exponential fits with base line for the FITC and RITC data respectively. In the inset the first part of the figure is enlarged.

developed.[27] For our studies however, this overlap of fluorescence in the detection ranges did not cause any difficulty in distinguishing between differently labeled particles (section 3D).

As is seen in Table 3 the extinction and emission maximas of RITC are shifted toward higher wavelengths after incorporation into the silica spheres (ca. 15 nm). The differences observed for the dye incorporated in SISOL and STSI are small (ca. 5 nm), although the 1-octadecanol-coated spheres have endured 16 h of heating at 190 °C. This is in contrast to the FITC-labeled spheres: hardly a shift was observed for incorporation of FITC in silica, but the coating reaction with 1-octadecanol caused a considerable red-shift in fluorescence[6] and the appearance of a new emission peak with a maximum at 385 nm.

The shapes of the excitation and absorption spectra of RITC were found to be similar, as is often found for this kind of dye.[13] The extinction coefficient was calculated based on absorption measurements of STSI in cyclohexane. A value of 2.2×10^6 $(M \cdot m)^{-1}$ was found using 60 g/mol for the molecular weight of silica and the incorporation efficiency of 49% of the starting amount of RITC, as was demonstrated in section 3A. This extinction coefficient gives an imaginary part of the refractive index $q = 2.6 \times 10^{-4}$. As was stated earlier this q value is too small to influence the scattering pattern in SLS. The extinction coefficients of RITC in sodium hydroxide solution (section 3A) and incorporated in silica (as determined here) are of the same order of magnitude.

The bleachability of RITC- and FITC-labeled spheres in the binary mixture FSA 7(3)/SISOL (see Table 1) has been measured with CSLM. The fluorescence intensity of FITC per pixel was almost twice as high as for RITC. This factor corresponds with the fact that for FITC in FSA 7(3),[17] on the one hand the amount of dye incorporated per particle was about 13 times higher than for RITC in SISOL and that on the other hand the FITC molecules in FSA 7(3) are distributed in a core with a volume that is almost 7 times larger than for the RITC molecules in SISOL (see Tables 4 and 2, respectively).

Table 4. Particle Properties of Rhodamine- and Fluorescein-Labeled Particles[a]

system	n_D	(λ) (nm)	ρ (g/mL)	N (molecules of fluorophore/ particle)	c (mol of fluorophore/ L of silica)
CORE				6.6×10^4	26×10^{-3}
SISOL	1.447	647	1.88	6.6×10^4	2.7×10^{-3}
Core of 4F-s				1.4×10^6	61×10^{-3}
4F-s	1.452		2.02	1.4×10^6	5.6×10^{-3}
FSA 7(3)				87×10^4	43×10^{-3}

[a] Refractive index (n_D), particle density (ρ), the amount of molecules fluorophore per particle (N), and fluorophore concentration per liter of silica (c) are given. Data for FITC-labeled particles 4D and 4F are taken from ref 6.

In Figure 5 the normalized fluorescence intensity of RITC- and FITC-labeled spheres is plotted versus exposure time. To obtain this bleaching curve each line scan was an average over four scans and the sample was illuminated with the wavelengths 488 and 568 nm (dual excitation) without attenuation filter. In the inset of Figure 5 part of the figure is enlarged. The shape of the curves was independent of the illumination intensity or the scan speed. Moreover, the decay in intensity measured with single excitation in samples containing only FITC-labeled or RITC-labeled spheres was equal to the results obtained in the binary system with dual excitation.

(27) Carlsson, K.; Mossberg, K. *J. Microsc.* **1992**, *167*, 23.

Apparently, the bleachability of both fluorophores is comparable. Initially, the intensity of RITC seems to decrease less than for FITC (inset), but it is only a slight difference. At larger exposure times the intensities even coincide. Even after 5000 scans the intensities still decrease, indicating that the intensity will finally approach zero. The decay cannot be fitted by a single exponential. A similar bleaching curve of FITC-labeled silica spheres was recently obtained in a fluorescence recovery after photobleaching study.[28] No further attempts have been made to fit the data, since the actual bleaching mechanism for the dye inside the silica spheres is not known. The data seem to indicate a complex bleaching mechanism and/or a distribution of molecules with different bleachabilities.

Based on these bleaching curves, it can be concluded that RITC-labeled spheres can also be studied with FRAP in order to determine the long-time self-diffusion coefficient. Preliminary measurements on the FRAP setup described in ref 12 have indeed corroborated this conclusion.

C. Dispersion Behavior. The STSI particles formed a stable dispersion in *cyclohexane*. Under gravity these spheres formed a sediment with a crystalline top layer of approximately 1 mm. After several months, the colloidal crystals had not grown larger. This behavior is exactly as has been reported before for monodisperse hard spheres with a radius around 200 nm.[25]

Dispersions of STSI in *chloroform* were also stable. Colloidal crystals formed spontaneously within minutes, filling the whole volume at volume fractions of approximately 7%. At somewhat lower volume fractions the growth rate became smaller and the final crystals, which were also smaller, were in equilibrium with a colloidal liquid phase. At volume fractions around 0.1% the sedimentation rate was several times lower than the calculated Stokes sedimentation rate of individual spheres. Taken together, these observations clearly indicate a particle charge, which is remarkable in rather apolar solvents such as chloroform.[4] However, because of the extreme low conductivity of chloroform (dielectric constant 4.8) electrophoresis measurements on the surface charge were unsuccessful.

In *hexadecane* the dispersions formed a voluminous gel at room temperature, which transformed into a stable dispersion at a temperature around 35 °C. This transition was reversible.

In *toluene* the system flocculated immediately. An increase in temperature did not result in a stable dispersion. This observation is contrary to what has been found for smaller 1-octadecanol-coated particles.[29] Probably, this is caused by the van der Waals forces which are stronger between these larger spheres. After addition of cyclohexane up to a total volume fraction of 50% in toluene, a stable dispersion was created, which displayed a phase transition into a concentrated and a dilute phase at approximately 5 °C. Possibly, the addition of cyclohexane reduces the van der Waals forces by reducing the refractive index between the silica and the solvent, to allow again the temperature-dependent phase separation as observed before.[29]

The binary mixture of small STSI and larger 4F-s spheres in chloroform (4F-s/STSI) formed an orange dispersion, which phase separated after a week into a pink upper fraction with orange fluorescence and a yellow-orange lower fraction with yellow-orange fluorescence separated by a sharp boundary. Based on color and fluorescence it was concluded that the homogeneous upper phase primarily consisted of the smaller rhodamine-labeled spheres, and the homogeneous lower phase consisted of both rhodamine- and fluorescein-labeled spheres. This was later confirmed by CSLM (see below). Although, there was also sedimentation during the time of observation, the appearance of the two phases was faster than the sedimentation of both dispersions in pure form at comparable concentrations. Therefore, the observed phenomenon is probably a phase separation in which most of the smaller RITC particles were expelled out of the phase of the larger FITC spheres, which formed the lower phase since it has a higher density. In capillaries filled with this mixture crystal reflections were observed, first in the lower fraction and later in the upper fraction, and these were examined with CSLM.

D. Fluorescence Confocal Scanning Laser Microscopy (CSLM). For dispersions in *cyclohexane* it appeared that the distance between the fluorescent cores of neighboring particles was too small to distinguish them separately in the bulk of the dispersion, both in the glasslike sediment and in the crystalline top layer. Only in the first layer of particles that were stuck onto the glass wall of the capillary was it possible to see touching particles as separate spheres, if the illuminating beam was positioned in such a way that no spheres deeper inside the sample were illuminated (thus, with part of the laser spot focused inside the glass wall). This clearly indicates that the lateral resolution is indeed about 200 nm, which is the size of the nonfluorescent silica layer of two touching particles. Consequently, the fact that particles from several layers were imaged in one plane, due to the lower resolution along the optical axis, made it hard to distinguish them in the bulk. The resolution might be improved by exciting the fluorophore with smaller wavelengths (e.g. 325 nm). Another possibility is a decrease in volume of the fluorescent core relative to the total volume of the sphere, in order to increase the distance between the fluorescent cores.

Micrographs of the gel of STSI in *hexadecane* were similar to those shown in refs 9 and 10, but here, as expected, the distance between the fluorescent CORES also appeared insufficient to distinguish separate spheres in the bulk of the gel phase.

Dispersions in *chloroform* could be studied with CSLM more easily due to a larger interparticle distance in the crystals caused by charge on the spheres. Dispersions with volume fractions of 7% crystallized within several minutes, as is depicted in Figure 6. The images were recorded respectively 55, 75, and 105 s after homogenization, showing the dynamics of a crystal growth process in the bulk of a dispersion (approximately 30 μm below the wall of the capillary). In the first image a random distribution is observed with a beginning of positional ordering in the lower right corner. The second image shows that the regular pattern increases from right to left, and in the last picture the spheres are ordered. It is emphasized that the crystal growth is observed in the bulk of the dispersion, and the orientation of the image plane is arbitrary. The spots that fluoresce more brightly than others are probably dumbbells, as can be observed in Figure 1b as well (denoted by an arrow). These spheres contain more fluorophore in the core than average STSI spheres. When the imaging spot hits a dumbbell, a voxel (three-dimensional picture element) is created with a higher intensity, because the

(28) Imhof, A.; van Blaaderen, A.; Maret, G.; Mellema, J.; Dhont, J. K. G. *J. Chem. Phys.* **1994**, *100*, 2170.
(29) Jansen, J. W.; de Kruif, C. G.; Vrij, A. *J. Colloid Interface Sci.* **1986**, *114* (2), 481.

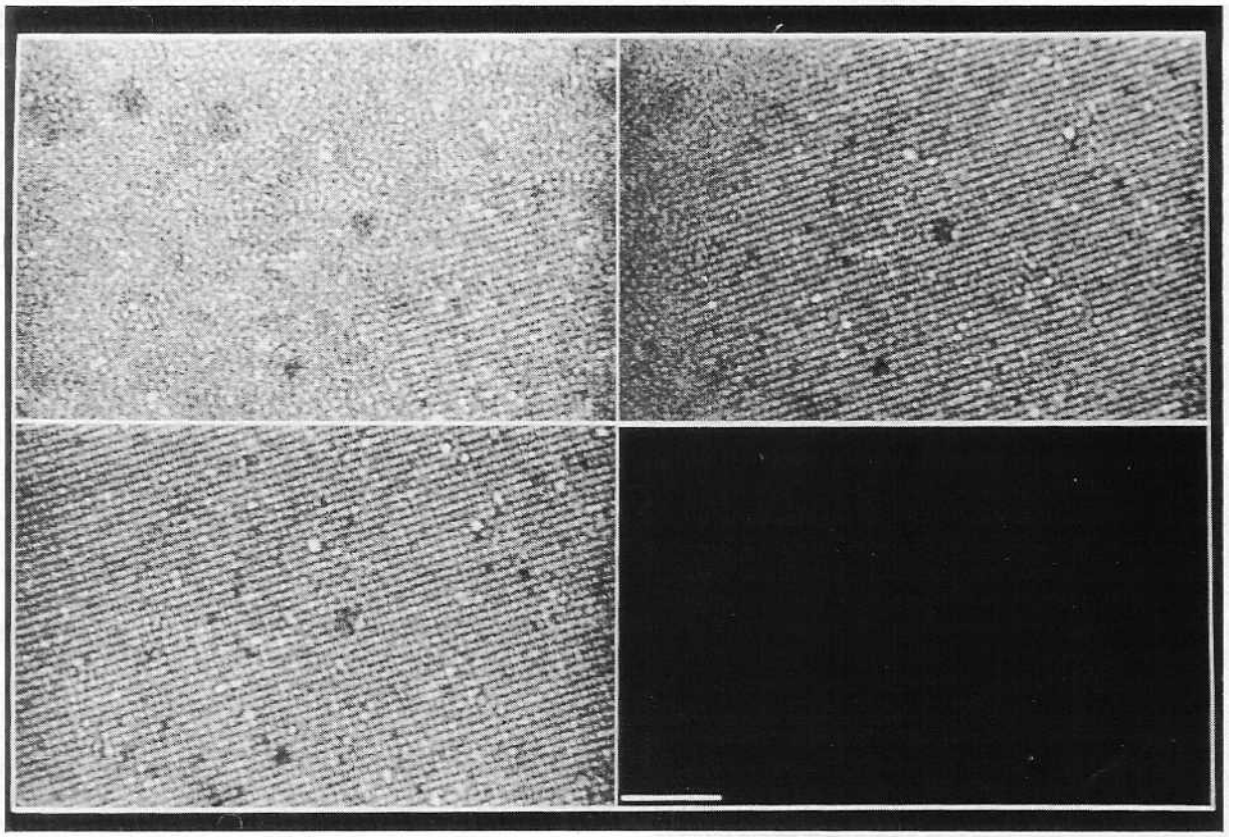

Figure 6. CSLM pictures of a homogeneous crystallization in a 7 vol % dispersion of STSI in chloroform. Parts a (top left), b (top right), and c (bottom left) were recorded respectively 55, 75, and 105 s after homogenization (bar = 25 μm). This image was recorded at approximately 30 μm below the glass wall of the capillary.

number of fluorophores excited is at most twice as large as in a single sphere. In the ordered phase of Figure 6, parts a and b, the same configuration of bright and dark spots can be recognized, indicating that the same cross section is observed in the three pictures and that systematic movements of the cuvette or dispersion on a micrometer scale were absent. Some point defects in the crystal lattice can also be recognized in the three images. The two large dark spots in the middle and in the middle lower part of the micrograph are probably dust particles. These first measurements clearly show that it is possible to follow crystallization dynamics with CSLM. An estimate can be made for the crystal growth rate (v) in this system by determining the velocity of the crystal/liquid interface in parts a and b of Figure 6. This growth rate of a crystal plane is about 4 μm/s: this value cannot be given with more accuracy, because the moving boundary shown in Figure 6 is a projection of a growing crystal plane with unknown orientation with respect to the imaging plane. This crystal growth rate can be compared to the theoretically predicted interface velocity of a molecular system, which was first proposed by Wilson[30] and Frenkel[31]

$$v = v_0\left(1 - \exp\left(\frac{-\Delta\mu}{k_B T}\right)\right) \qquad (2)$$

Here v_0 is related to kinetic behavior at the crystal surface, and the term between parentheses is a statistical sticking factor determined by $(\Delta\mu/k_BT)$, in which $\Delta\mu$ is the difference in chemical potential between liquid and crystalline state and k_BT is the thermal energy. Since $\Delta\mu$ has an unknown value, and the volume fraction of the dispersion shown in Figure 6 was chosen because it had the highest crystallization growth rate, the observed rate is compared with the maximum value as given by eq 2. Aastuen *et al.*[32] who also used eq 2 for a colloidal system proposed to equate v_0 to the mean velocity of a Brownian particle over the mean interparticle distance ζ

$$v_0 = \frac{4D_0}{\zeta} \qquad (3)$$

here D_0 is the free Stokes diffusion coefficient for a single particle (hydrodynamic interactions are less important for charged systems). For the STSI system in chloroform D_0 is equal to 2.0×10^{-12} m^2/s (see Figure 3), and the minimum ζ is assumed to be approximately 850 nm, i.e. the distance between two spheres in chloroform, as will be discussed later. Therefore, the maximum rate of crystal growth is predicted to be 10 μm/s, which is of the same order of magnitude as the observed growth rate. It seems therefore, that the dynamics of colloidal crystal growth in these charged systems are reasonably described by eq 3.

Another point of interest is the coexistence of a disordered and an ordered phase in the bulk of the STSI dispersion in chloroform (approximately 30 μm below the wall of the capillary) at a somewhat lower volume fraction, as shown in Figure 7. It is emphasized that the studied dispersion had reached the equilibrium stage, because this configuration remained stable longer than several hours. In parts a and b of Figure 7 the same optical sectioning is displayed, but integrated over respectively two and ten scans. In the two figures a regular pattern can be seen, both on the right side and in the upper left corner. These patterns come from different crystal planes: on the right side a hexagonal closest packing is recognized. Between the two crystals a disordered structure is found, which becomes vague if integrated over a longer period of time.

(30) Wilson, H. A. *Philos. Mag.* **1900**, *50*, 238.
(31) Frenkel, J. *Phys. Z. Sowjetunion* **1932**, *1*, 498.

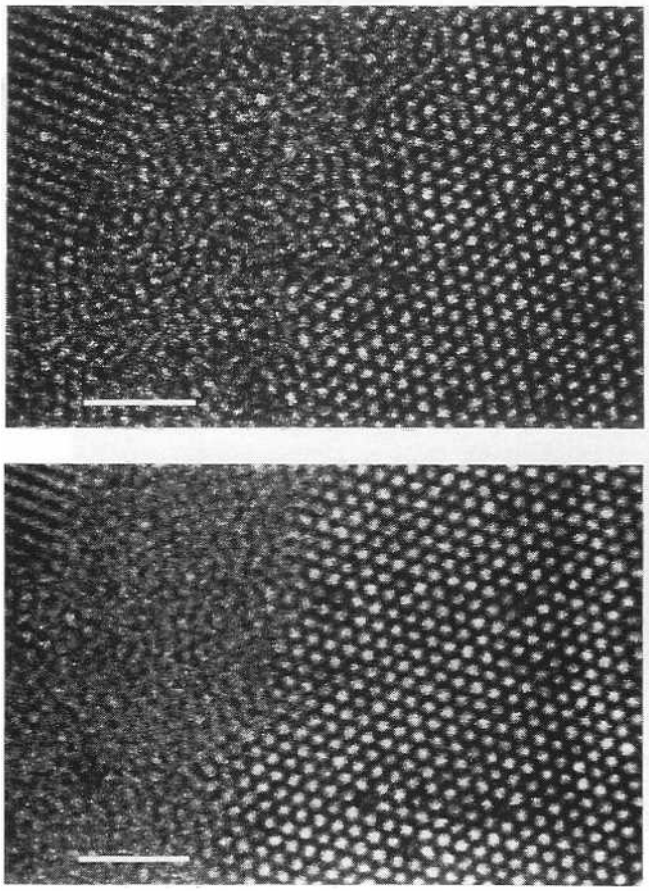

Figure 7. CSLM graphs of an equilibrium coexistence between a liquid and two crystalline phases in a 7 vol % dispersion of STSI in chloroform (30 μm below the glass wall of the capillary). Parts a (top) and b (bottom) are integrated over respectively two and ten scans. The bar represents 5 μm.

As expected, the spheres in the ordered phase are fixed near a lattice position (resulting in a better contrast after averaging over several frames), while the spheres in the disordered, fluid phase are mobile (resulting in a decrease of the contrast). The interface between the liquid and the crystal does not seem to follow a well-defined crystal plane, and apparently the system is already above its roughening transition, as was required by Aastuen *et al.*[32] Along the interface there was a layer with a width of three spheres approximately, which could belong either to the crystal or to the liquid phase. The fact that there is indeed no correlation between orientations of two crystals neighboring the thin liquid phase indicates that there is no influence of the wall of the capillary. This appears to be the first observation, on a particle level, of a boundary between an equilibrium coexistence of a liquid-like and crystalline phase in the bulk of a dispersion. A quite similar boundary which has been observed earlier by Hachisu was clearly influenced by the wall of the capillary.[33]

The interparticle distance a in this colloidal crystal is defined as the distance between the centers of the neighboring particles in the closest packed plane depicted in Figure 7. This distance a was determined to be 846 nm, which is considerably larger than twice the particle radius of 215 nm. This size difference is partly caused by the fact that the spheres also crystallize at volume fractions lower than required for a touching closest packed system, analogous to hard spheres which crystallize already at volume fractions lower than 74%. A hard sphere system starts to crystallize at a volume fraction of 49% and is fully crystalline at volume fractions of 55% (Kirkwood–Alder transition[34]). Only at $\phi = 74\%$ the spheres are actually touching each other. Assuming a closest packed crystal structure for the colloidal crystals in chloroform (e.g. face centred cubic: fcc) and using a sphere radius (r) of 215 nm, the volume fraction ϕ of the crystal phase is calculated as: $\phi = (4\sqrt{2}\pi/3)\cdot(r/a)^3$. With an interparticle distance (a) of 846 nm, a volume fraction ϕ of 9.7% is obtained. This smaller volume fraction compared to 55% for hard sphere systems is a clear indication of a charged system. An explanation for the difference between the calculated value and the originally prepared volume fraction of 7% might be the fact that not all the particles have crystallized, analogous to the difference between the crystallization point at 49 vol % and the melting point at 55 vol % for hard spheres. Scaling these hard sphere crystallization and melting volume fractions respectively to these soft sphere volume fractions can only account for an increase in volume fraction of approximately 1%. However, it has been observed before that the liquid-crystalline coexistence region for soft spheres is larger than expected from this mapping.[28] At present it is attempted to obtain the crystallization and melting concentrations for the STSI dispersion in chloroform more accurately. Furthermore, light scattering data on the colloidal crystal structure are compared to results obtained with CSLM.

The mixture of rhodamine-labeled STSI and fluorescein-labeled 4F-s was studied with CSLM, just after preparation and 2 weeks after preparation. In the former case (Figure 8) no phase separation was observed. Parts a and b of Figure 8 show respectively the FITC (green) and RITC (red) detector output of the mixture situated at the glass wall. Both fluorophores are excited and detected simultaneously. It appeared that the RITC-labeled particles were fluorescing much stronger than the FITC-labeled spheres in this case (compare to the bleaching experiments described in section 3B). Therefore, the amplification of the PMT signal for FITC had to be increased. As a result, the emission of RITC could be vaguely detected in the FITC channel as well, as was predicted while discussing Figure 4. This can be seen clearly in Figure 8c which is composed of both parts a and b of Figure 8. The color of the RITC spots is orange compared to the red spots in Figure 8b, indicating that these spots are a combination of vaguely colored green spots in Figure 8a and red spots in 8b. The RITC and FITC spheres are randomly distributed without any ordering, and the positions of the rhodamine and fluorescein spheres can be identified easily. Although there is a size difference in fluorescent cores of 200 nm, the spots in Figure 8c seem to be of similar size. This can be explained by assuming that the interaction potential of the smaller RITC spheres allows for Brownian movements with a larger amplitude than that of the larger FITC spheres.

Figure 9 shows that the lower fraction of the phase separated system, taken 15 days after Figure 8, is now dominated by fluorescein-labeled particles. In this fraction crystal reflections were observed visually. Figure 9 shows a superposition of the images recorded by both PMT's. The depicted image was situated at approximately 20 μm below the wall of the capillary. Three remarks are made. First, the fluorescein spheres are positioned in a regular pattern, in which a hexagonal closest packing can be recognized. This corresponds to the visual observation of

(32) Aastuen, D. J. W.; Clark, N. A.; Cotter, L. K.; Ackerson, B. J. *Phys. Rev. Lett.* **1986**, *57* (14), 1733.

(33) Israelachvili, J. *Intermolecular and surface forces*, 2nd ed.; Academic Press: London, 1992; pp 92–93.

(34) Hoover, W. G.; Ree, F. H. *J. Chem. Phys.* **1968**, *49*, 3609.

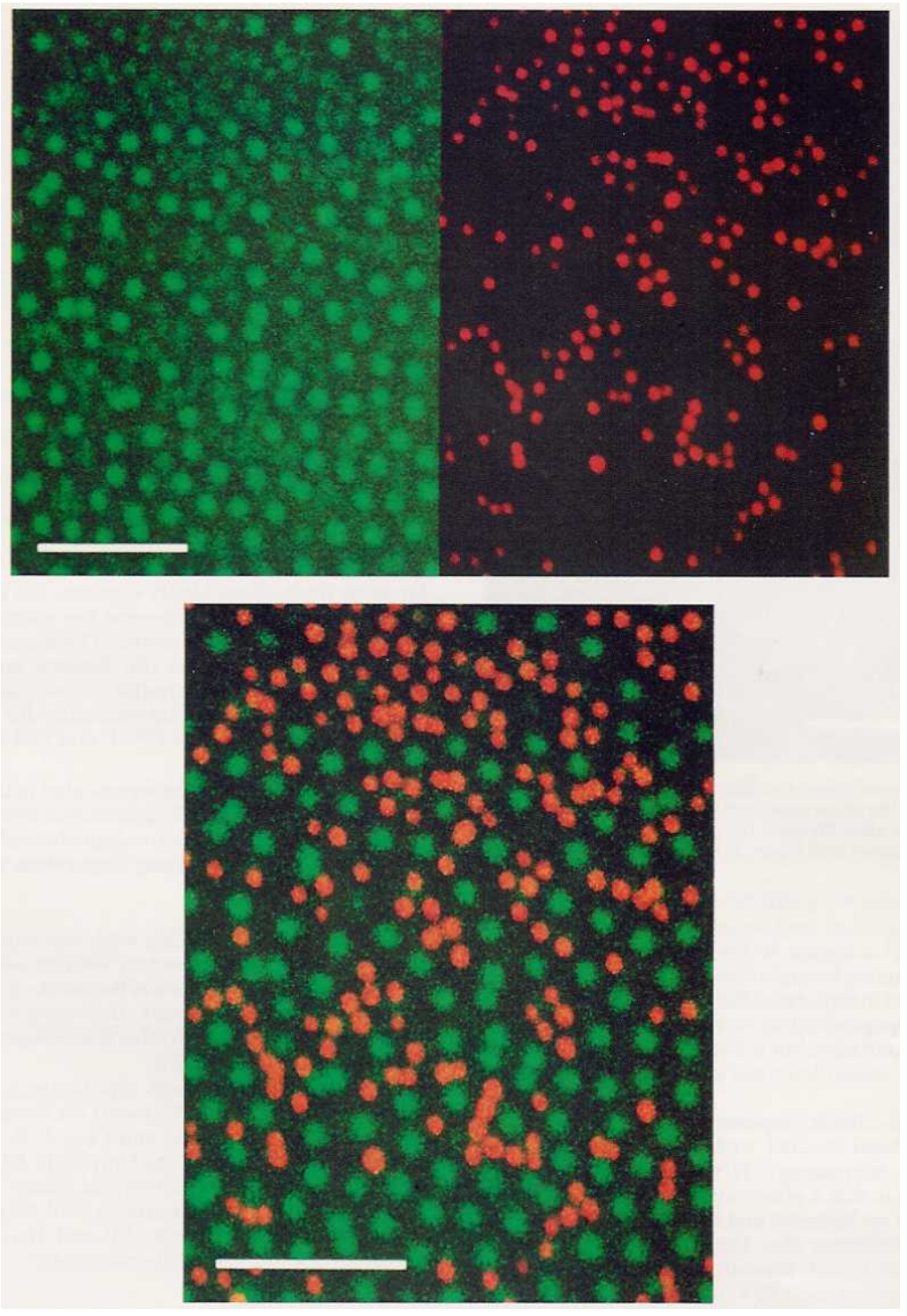

Figure 8. CSLM graphs of the just prepared dispersion of the binary mixture 4F-s/STSI containing fluorescein and rhodamine labeled spheres in chloroform (just below the glass wall of the capillary). Both fluorophores were excited and detected simultaneously in the dual excitation mode. The bar represents 5 μm. In parts a and b (top left, top right) the separate images of, respectively, fluorescein and rhodamine are shown. Part c (bottom) is a combination of parts a and b.

crystal reflections. Second, the number of rhodamine spheres has decreased compared to the system displayed in Figure 8, which agrees with the observed phase separation. Third, the rhodamine-labeled spheres still present in this fluorescein dominated fraction either fit into lattice positions of the FITC crystal without actually disturbing the crystallinity (e.g. in the middle, left part of the image) or are situated on interstices where they disturb the lattice (e.g. in the upper part of the image). Further work is required to determine the difference in interaction potentials of these particles in chloroform in order to get a better understanding of the phase behavior in this bidisperse system. The thin upper crystal fraction could not be studied, since this top layer was destroyed too easily by gravity after placing the capillary in a horizontal position as was necessary for microscopic observation.

Summary and Conclusions

A fluorescent model system of monodisperse silica spheres labeled with the dye rhodamine isothiocyanate has been synthesized and characterized for the first time. The fluorophore has been incorporated into an organosilica core with a radius of 100 nm on to which a silica layer of 100 nm has been grown. Rhodamine-labeled spheres could

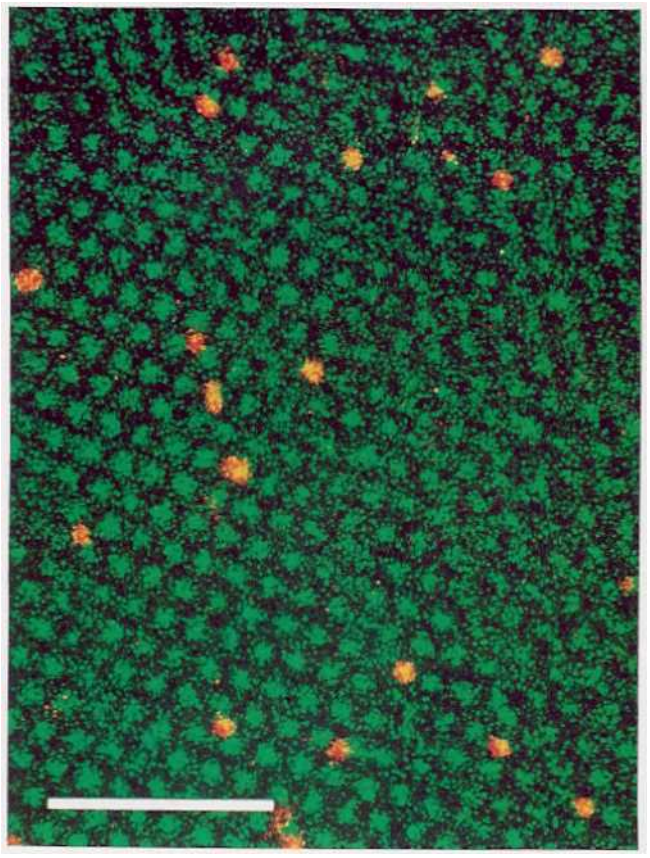

Figure 9. Dual excitation and detection CSLM graph of the lower fraction of the phase separated binary mixture 4F-s/STSI, recorded 15 days after Figure 8 (20 μm below the glass wall of the capillary; compare with Figure 8c). The bar represents 5 μm.

stand high temperatures (200 °C) better than fluorescein-labeled spheres, since they could be coated with 1-octadecanol without a change in fluorescence. The bleachability of rhodamine incorporated in silica appeared to be similar to that of incorporated fluorescein. The bleaching effect is not strong enough to cause any problem with the imaging of the particles, but it does make it more difficult to use the fluorescent intensity as a measure for colloid concentration.

Concentrated colloidal dispersions of rhodamine labeled spheres have been studied with fluorescence confocal scanning laser microscopy. It was found by studying colloidal crystals and a glassy state of the hard-sphere-like particles in cyclohexane and the thermotropic reversible gel in hexadecane that the lateral resolution was sufficient to distinguish touching spheres, but that the nonfluorescent silica layer (2 × 100 nm) was too thin for the axial resolution to image the spheres separately. These findings are in accordance with the theoretical lateral resolution of about 200 nm and an axial resolution of 650 nm.[35] The interparticle distance of the spheres in colloidal crystals in chloroform (850 nm) was sufficient to depict the particles separately as was illustrated by micrographs of an equilibrium interface between a colloidal crystal (of which exactly one close packed crystal plane was depicted) and a colloidal liquid phase. Currently it is attempted to establish the crystal structure of these colloidal crystals with CSLM in more detail, and these results are being compared with light scattering. However, it is already clear from the first preliminary results that the CSLM data complement scattering data. For instance in a time-resolved light scattering study[36] it appeared not possible to measure an absolute crystal growth rate, which was for this similar colloidal system easily obtained by CSLM (4 μm/s). Further, the number of crystallites and their size polydispersity are certainly within the range of the technique and very difficult to obtain through scattering studies.

Micrographs of binary dispersions of FITC and RITC labeled spheres in chloroform clearly indicated that with dual excitation and detection CSLM allows for the simultaneous detection of both types of particles in one measurement. With (light) scattering this can only be accomplished with a series of contrast variation studies. By using filters these binary mixtures can also be used in FRAP experiments to measure the exchange diffusion between the different particles. The binary mixtures are also well suited to obtain the dynamic structure factor with fluorescence cross correlation spectroscopy,[3] because the laser intensities that are used with this technique are so much lower than with FRAP and CSLM (e.g. 10 000 times).

Finally, the measurements presented in this paper have shown that confocal scanning laser microscopy has yielded interesting results on structural and dynamical properties of concentrated, crystallizing dispersions of rhodamine-labeled silica spheres.

Acknowledgment. This work was supported by the *Stichting voor Fundamenteel Onderzoek der Materie* (Foundation for Fundamental Research on Matter) which is part of the *Nederlandse Organisatie voor Wetenschappelijk Onderzoek* (Netherlands Organization for the Advancement of Research).

We thank Willem Hage (Netherlands Institute for Developmental Biology, Utrecht) for his assistance with the CSLM measurements and Cees J. R. van der Oord (Department of Biophysics, University Utrecht) for the fluorescence spectra. Further, we thank Arnout Imhof for supplying us with the particles FSA 7(3) and, together with Jeroen S. van Duijneveldt and Henk N. W. Lekkerkerker, for stimulating discussions and a critical reading of the manuscript.

(35) Hell, S.; Reiner, G.; Cremer, C.; Stelzer, E. H. K. *J. Microsc.* **1993**, *169* (3), 391.

(36) Dhont, J. K. G.; Smits, C.; Lekkerkerker, H. N. W. *J. Colloid Interface Sci.* **1992**, *152* (2), 386.